Structural Characterization of the Manganese Sites in the Photosynthetic Oxygen-Evolving Complex Using X-ray Absorption Spectroscopy

James E. Penner-Hahn,*,† Richard M. Fronko,† Vincent L. Pecoraro,*,† Charles F. Yocum,*,‡,† Scott D. Betts,‡ and Neil R. Bowlby‡

Contribution from the Department of Chemistry, University of Michigan, Ann Arbor, Michigan 48109-1055, and Department of Biology, University of Michigan, Ann Arbor, Michigan 48109-1048. *Received February 22, 1989*

Abstract: Manganese X-ray absorption spectra (XAS) are reported for the S_1 state of highly purified, highly concentrated preparations of the oxygen-evolving complex (OEC) from photosystem II (PSII). Improvements in concentration (ca. 1.5 mM Mn) and detection efficiency (13-element solid-state detector array) have permitted a substantial improvement in data quality relative to previous solution XAS studies of PSII. Principal findings are that there is no need to include a shell of oxygens at ca. 1.75 Å in order to account for the Mn EXAFS, that there are 2–3 Mn–Mn distances of ca. 2.7 Å, and that there are one and possibly two shells of additional scatterers at longer distance (ca. 3.3 and 4.2 Å) from the Mn. Even with this higher quality data, it is not possible to use EXAFS to determine whether chloride is coordinated to the Mn. The structural consequences of these results are discussed in the context of proposed structural models. It is concluded that neither a cubane nor previously prepared butterfly type clusters can account for the observed features. Although EXAFS alone cannot uniquely determine the structure of the OEC, the present data together with other physical observations suggest an alternate model for the OEC consisting of a trinuclear Mn cluster together with a mononuclear Mn. A new approach for interpreting X-ray absorption near edge structure (XANES) spectra by using edge shape rather than only the energy of the first inflection point is presented. This method correctly determines the Mn(II) concentration in crystallographically characterized mixed-valence Mn trimers. The OEC XANES spectrum is unusually broad, and the edge fitting method suggests that one interpretation of this broad edge is the presence of mixed-valence Mn(II/III/III/IV) in the S_1 state. The XANES and EXAFS data taken together point to a manganese environment which is more heterogeneous than previously appreciated.

The biological production of dioxygen and the subsequent metabolism of this molecule and its reduced forms (O_2^{n-}) are among the most important classes of reactions in the biosphere. Nearly all of the dioxygen which animals and aerobic bacteria use during respiration originates from the photosynthetic oxygen-evolving complex (OEC) which is found in the chloroplast thylakoid membranes of higher plants and algae. The OEC catalyzes the reaction shown in eq 1.[1] Photosynthetic membranes

$$2H_2O \rightarrow O_2 + 4\,H^+ + 4e^- \qquad (1)$$

which are illuminated with short, saturating flashes of light evolve oxygen after four flashes starting with the third flash,[2] thus demonstrating that each photosystem II (PSII) reaction center acts independently to acquire sequentially four oxidizing equivalents. The five kinetically resolvable intermediates are designated S_0 to S_4 with S_0 being the most reduced level.[2] The stable, dark adapted form of the enzyme is predominantly S_1.[3]

Four specifically bound Mn are required for OEC activity.[4] Dismukes and Siderer[5] have detected at low temperatures a multiline EPR signal centered at $g \approx 2$ (≈19 lines spread over a 1900 G range) associated with the S_2 state. The multiline signal directly implicates a multinuclear manganese cluster in the catalytic process.[6,7] More recently, a second EPR spectral feature from S_2 has been observed at $g_{eff} \approx 4$ under conditions of illumination which inhibit multiline signal formation.[8]

Interpretation of these spectroscopic signatures has fueled considerable controversy. Initially, the multiline signal was assigned to a mixed-valence dinuclear Mn site.[5] Subsequently, Brudvig and co-workers suggested that the two S_2 EPR signals could be assigned to different conformations of a mixed-valence tetranuclear cluster.[9,10] More recently, Hansson et al.[11] have reinterpreted these spectra by using a model that incorporates a mononuclear Mn(IV) (an $S = 3/2$ spin manifold that is the origin of the $g_{eff} \approx 4$ signal) in electron-transfer equilibrium with a mixed-valence cluster (an $S = 1/2$ spin system that provides the multiline component). In this model, the mixed-valence cluster could be dinuclear, in which case the stoichiometry would require the presence of an additional EPR nondetectable mononuclear center or the mixed-valence cluster could be trinuclear.[12,13]

X-ray absorption spectroscopy (XAS) can provide useful structural information for metalloenzyme active sites.[14] Extended X-ray absorption fine structure (EXAFS) spectra can be analyzed to give bond lengths with a precision of 0.02 Å for nearest neighbors and ca. 0.05 Å for more distant atoms. The precision

* Authors to whom correspondence should be addressed.
† Department of Chemistry.
‡ Department of Biology.

(1) For recent reviews, see: (a) Babcock, G. T. *New Comprehensive Biochemistry, 15, Phytosynthesis*; Amasz, J., Ed.; Elsevier: Amsterdam, 1987. (b) Pecoraro, V. L. *Photochem. Photobiol.* **1988**, *49*, 249. (c) Renger, G. *Angew. Chem., Int. Ed. Engl.* **1987**, *26*, 643–660.
(2) Kok, B.; Forbush, B.; McGloin, M. *Photochem. Photobiol.* **1970**, *11*, 457.
(3) Styring, S.; Rutherford, A. W. *Biochemistry* **1987**, *5*, 2401.
(4) Cheniae, G. M.; Martin, I. F. *Biochim. Biophys. Acta* **1970**, *197*, 219–239.
(5) (a) Dismukes, G. C.; Siderer, Y. *FEBS Lett.* **1980**, *212*, 78–80. (b) Dismukes, G. C.; Siderer, J. *Proc. Natl. Acad. Sci. U.S.A.* **1981**, *78*, 274.
(6) Zimmerman, J. L.; Rutherford, A. W. *Biochim. Biophys. Acta* **1984**, *767*, 160–167.
(7) Brudvig, G. W.; Casey, J. L.; Sauer, K. In *The Oxygen Evolving System of Photosynthesis*; Inoue, Y., et al., Eds.; Academic Press: Tokyo, 1983; pp 159–164.
(8) Casey, J.; Sauer, K. *Biochem. Biophys. Acta* **1984**, *767*, 21.
(9) Brudvig, G. W.; Crabtree, R. H. *Proc. Natl. Acad. Sci. U.S.A.* **1986**, *83*, 4586.
(10) de Paula, J. C.; Beck, W. F.; Brudvig, G. W. *J. Am. Chem. Soc.* **1986**, *108*, 4002.
(11) Hansson, O. R.; Aasa, R.; Vanngard, T. *Biophys. J.* **1987**, *51*, 825.
(12) Li, X.-H.; Kessissoglou, D. P.; Kirk, M. L.; Bender, C. A.; Pecoraro, V. L. Inorg. *Chem.* **1988**, *27*, 1.
(13) Kessissoglou, D. P.; Kirk, M. L.; Bender, C. A.; Lah, M. S.; Pecoraro, V. L. *J. Chem. Soc., Chem. Commun.* **1989**, 87.
(14) For reviews, see: (a) Lee, P. A.; Citrin, P. H.; Eisenberger, P.; Kincaid, B. M. *Rev. Mod. Phys.* **1981**, *53*, 769–806. (b) Powers, L. *Biochim. Biophys. Acta* **1982**, *683*, 1–38. (c) Scott, R. A. *Methods Enzymol.* **1985**, *107*, 414–459. (d) Cramer, S. P. In *X-ray Absorption: Principles, Applications, and Techniques of EXAFS, SEXAFS, and XANES*; Koningsberger, D. C., Prins, R., Eds.; Wiley-Interscience: New York, 1988; pp 257–320. (e) Teo, B. K. *EXAFS: Basic Principles and Data Analysis*; Springer-Verlag: New York, 1986.

0002-7863/90/1512-2549$02.50/0

in coordinate number is ca. ±25% and the uncertainty in atomic number approximately ±10. The latter constraint results in an ambiguity in ligation in so far as N and O, S and Cl, or Mn, Fe, and Ca cannot be distinguished.

In a series of studies,[15-21] Klein, Sauer and co-workers found that the average Mn coordination environment includes a Mn–(N,O) distance of 1.75–1.8 Å, a disordered shell of oxygens and/or nitrogens at an average distance of 2.15 Å from the Mn, and a Mn–(Mn or Fe) distance of 2.7 Å. The shorter Mn–(N,O) distance has been assigned to a bridging ligand based on comparison with dinuclear manganese model complexes, while the longer distance is believed to be due to terminal nonbridging nitrogen and/or oxygen ligands. The observed Mn–Mn distance of 2.7 Å provides additional evidence that at least two manganese ions are in close proximity. Thus, these EXAFS data show that the OEC must contain at least a dinuclear cluster and are consistent with, but not proof of, the existence of a higher nuclearity cluster.

In addition to uncertainty over the nuclearity, the oxidation states of the manganese cluster are still unclear. The multiline EPR signal has been attributed to μ-oxo-bridged Mn(III/IV)[22] and Mn(II/III)[23] dimers based on line shape analysis of the signal; however, assignment of oxidation states based only on the manganese hyperfine interactions is difficult.[24] The former is consistent with results from X-ray absorption near edge structure (XANES). On the basis of X-ray edge energies, the average OEC oxidation state for S_1 has been assigned as Mn(III) with one or more manganese being oxidized on conversion to S_2.[17]

Inorganic cofactors other than manganese are also required for O_2 production. Membranes depleted of chloride[25,26] or calcium[27,28] lose the capacity to produce dioxygen and do not undergo complete S state advancement. On the basis of analyses of inhibition kinetics induced by primary amines. Sandusky and Yocum have postulated that chloride ion forms a bridge between manganese ions to mediate electron transfer.[29,30] This amine/Cl competition has been confirmed in EPR studies by Brudvig and co-workers.[31] It was originally reported that the EXAFS data could not be fitted to accommodate chloride as a manganese ligand in either S_1 or S_2;[21a,32] however, this claim has since been moderated.[20]

Two to three calcium ions are bound to PSII.[33] In addition to being required for S state advancement and oxygen production, calcium can reconstitute activity in salt-washed membranes where the extrinsic 23 and 17 kDa peptides have been depleted.[27] These and other data suggest that calcium may play an important structural role in the OEC. It is quite possible that the location of the bound calcium may be at or near the active site.

The recently reported procedure for isolating PSII reaction centers by using the detergent octylglucopyranoside in a high ionic strength buffer has permitted the preparation of highly purified, highly concentrated samples of the OEC.[34] This procedure separates the PSII reaction centers from the rest of the photosynthetic membrane and permits preparation of samples containing ≈1.5 mM Mn (400 μM reaction centers). This is significantly more concentrated than samples which have previously been examined by XAS and thus has permitted us to obtain data having a significantly enhanced signal-to-noise ratio.

We report herein X-ray absorption studies of the S_1 state of the OEC by using these highly resolved core preparations. The specific questions addressed are the manganese cluster nuclearity, the identity of the ligands to the manganese, and the oxidation states of the manganese in S_1. We conclude that XAS data alone cannot uniquely define the structure of the manganese cluster; however, these data in conjunction with other observations can be used to rule out many of the existing structural proposals. Most importantly, our present data provide a picture of a very heterogeneous environment for the manganese, suggesting a system of greater structural complexity than has previously been considered.

Table I. Edge Energies for Mn Models Compounds

model[a]	valence[b]	edge energy (eV)[c]	ref
$[Mn(SALPS)_2]_2$	+2	6547.1	37
$Mn(C_3H_4N_2)_6Cl_2$	+2	6547.2	38
$Mn(AcO)_4 \cdot 6H_2O$	+2	6548.6	39
$Mn_3(SALADHP)_2(AcO)_4(MeOH)_2$	+2.67	6549.6	12
$Mn_3(SALADHP)_2(AcO)_4(pyrOH)_2 \cdot 2H_2O$	+2.67	6549.6	40
$Mn_3(SALADHP)_2(AcO)_4(H_2O)_2$	+2.67	6549.8	40
$[Mn_2(DALAP)(DMF)_2]$	+3	6550.5	41
[Mn[(2-OH)SALPN](AcO)]	+3	6550.4	42, 43
Mn(TMP)(Cl)	+3	6550.6	44
$\{NaMn_2[(2\text{-}OH)SALPN]\}_2(AcO)_4$	+3	6550.7	42, 43
$\{Mn[(2\text{-}OH)\text{-}5\text{-}Cl\text{-}SALPN]\}_2CH_3OH$	+3	6551.2	42, 43
$Mn[OC(NH_2)_2]_6(ClO_4)_3$	+3	6551.5	45
$[Mn(SALAHP)(AcO)]_2$	+3	6552.2	46
$Mn(C_5H_7O_2)_3$	+3	6552.9	47
$Mn(TPP)(OMe)_2$	+4	6552.1	48
$Mn(SALADHP)_2$	+4	6554.2	49, 50
$[Mn(SALPN)O]_2$	+4	6554.6	51
OEC, S_1 state		6549.9	

[a] See footnote 40 for abbreviations. [b] Average formal oxidation state of Mn. [c] Edge energy defined as the energy of the first inflection point on the rising edge. Within each oxidation state, compounds are sorted by increasing edge energy.

Experimental Section

Sample Preparation. Highly purified samples of the OEC were prepared according to the procedure of Ghanotakis et al.[34] Specific activity was 1400 μmol of O_2/(h-mg of chlorophyll)$^{-1}$. Samples were estimated to be 1.5 mM in Mn based on chlorophyll content and previously determined chlorophyll:Mn ratios.[34] Samples contained no adventitious

(15) Kirby, J. A.; Robertson, A. S.; Smith, J. P.; Thompson, A. C.; Cooper, S. R.; Klein, M. P. *J. Am. Chem. Soc.* **1981**, *103*, 5529–5537.
(16) Kirby, J. A.; Goodin, D.; Wydrynski, T.; Robertson, A. S.; Klein, M. P. *J. Am. Chem. Soc.* **1981**, *103*, 5537–5542.
(17) (a) Goodin, D.; Yachandra, V. K.; Britt, R. D.; Sauer, K.; Klein, M. P. *Biochim. Biophys. Acta* **1984**, *767*, 209–216. (b) Cole, J.; Yachandra, V. K.; Guiles, R. D.; McDermott, A. E.; Britt, R. D.; Dexheimer, S. L.; Sauer, K.; Klein, M. P. *Biochim. Biophys. Acta* **1987**, *890*, 395–398.
(18) Yachandra, V. K.; Guiles, R. D.; McDermott, A.; Britt, R. D.; Dexheimer, S. L.; Sauer, K.; Klein, M. P. *Biochim. Biophys. Acta* **1986**, *850*, 324–332.
(19) Cole, J. L.; Yachandra, V. K.; McDermott, A. E.; Guiles, R. D.; Britt, R. D.; Dexheimer, S. L.; Sauer, K.; Klein, M. P. *Biochemistry* **1987**, *26*, 5967–5973.
(20) Yachandra, V. K.; Guiles, R. D.; McDermott, A.; Cole, J. L.; Britt, R. D.; Dexheimer, S. L.; Sauer, K.; Klein, M. O. *Biochemistry* **1987**, *26*, 5974–5981.
(21) (a) Yachandra, V. K.; Guiles, R. D.; McDermott, A.; Britt, R. D.; Cole, J.; Dexheimer, S. L.; Sauer, K.; Klein, M. P. *J. Phys. Colloq. (Paris)* **1986**, *47*, C8/1121–C8/1128. (b) McDermott, A. E.; Yachandra, V. K.; Guiles, R. D.; Cole, J. L.; Dexheimer, S. L.; Britt, R. D.; Sauer, K.; Klein, M. P. *Biochemistry* **1988**, *27*, 4021–4031.
(22) Dismukes, G. C.; Ferris, D.; Watnick, P. *Photochem. Photobiophys.* **1982**, *3*, 243–256.
(23) Andreasson, L.-E.; Hansson, O.; Vanngard, T. *Chem. Scr.* **1983**, *21*, 71–74.
(24) Mabad, B.; Tuchagues, J.-P.; Hwang, Y. T.; Hendrickson, D. N. *J. Am. Chem. Soc.* **1985**, *107*, 2801–2802.
(25) Theg, S.; Jursinic, P.; Homann, P. H. *Biochim. Biophys. Acta* **1984**, *766*, 636.
(26) Itoh, S.; Yerkes, C. T.; Koike, H.; Robinson, H. H.; Crofts, A. R. *Biochim. Biophys. Acta* **1984**, *766*, 612–622.
(27) Ghanotakis, D. F.; Babcock, G. T.; Yocum, C. F. *FEBS Lett.* **1984**, *167*, 127.
(28) Ghanotakis, D. F.; Topper, J. N.; Babcock, G. T.; Yocum, C. F. *FEBS Lett.* **1984**, *170*, 169–173.
(29) Sandusky, P. O.; Yocum, C. F. *Biochim. Biophys. Acta* **1984**, *766*, 603–611.
(30) Sandusky, P. O.; Yocum, C. F. *Biochim. Biophys. Acta* **1986**, *849*, 85–93.
(31) Beck, W. A.; Brudvig, G. W. *Biochemistry* **1986**, *25*, 6479–6486.
(32) (a) Yachandra, V. K.; Guiles, R. D.; McDermott, A.; Cole, J.; Britt, R. D.; Dexheimer, S. L. In *Progress in Photosynthesis Research*; Biggens, J., Ed.; Nighoff: Dordrecht, 1987; Vol. 1, pp 557–560. (b) McDermott, A.; Yachandra, V. K.; Guiles, R. D.; Britt, R. D.; Dexheimer, S. L.; Sauer, K.; Klein, M. P. In *Progress in Photosynthesis Research*; Biggens, J., Ed.; Nighoff: Dordrecht, 1987; pp 565–568.
(33) Carumata, K.; Chenaie, G. M. *Plant Phys.* **1987**, *84*, 587.
(34) (a) Ghanotakis, D. F.; Yocum, C. F. *FEBS Lett.* **1986**, *197*, 244. (b) Ghanotakis, D. F.; Demetrious, D. M.; Yocum, C. F. *Biochim. Biophys. Acta* **1987**, *891*, 15–21.

Mn(II) as judged by EPR at liquid He temperatures in the presence of excess Ca^{2+}. Two samples in the S_1 state were loaded into Lucite EXAFS cells and stored at 77 K. All X-ray absorption measurements were made at 10 K by using an Oxford Instruments Cryostat (CF-1204). XAS data for the two OEC samples were measured over the range 6432–7116 eV for a total of 9 and 6 h, respectively. Data were measured at SSRL beam line 7-3 by using a Si(400) double crystal monochromator and were recorded as fluorescence excitation spectra by using a 13-element high-purity Ge detector[35] to monitor X-ray fluorescence.

Synthetic manganese complexes having well-characterized oxidation states, coordination geometries, and variable nuclearities were used as models for the OEC edge structure. The models which were studied are summarized in Table I.[36] The preparation and characterization of these models are described elsewhere.[12,13,37-51] Spectra of the model compounds were measured in transmission mode by using finely ground powders suspended in a BN matrix.

Data Analysis. Energy calibration was accomplished by using $KMnO_4$ as an internal standard,[14c] with the maximum in the $KMnO_4$ pre-edge peak assigned as 6543.3 eV.[17a] Energies were converted from eV to photoelectron wave vector $k = (h/2\cdot\pi)^{-1}[2m_e(E - E_0)]^{1/2}$ by using a threshold energy $E_0 = 6555$ eV. EXAFS data analysis followed standard procedures for pre-edge background removal, spline fitting, and Fourier transformation.[14] In brief, the pre-edge absorption was modelled by a second-order polynomial fitted over a 300-eV region below the absorption threshold, and the extrapolated pre-edge polynomial was subtracted from the entire range of data. The EXAFS $\chi(k)$ is defined as $(\mu - \mu_0)/\mu_0$ where μ_0 is the absorption in the absence of EXAFS effects. Since μ_0 cannot be directly measured, we approximate the EXAFS as $(\mu - \mu_s)/\mu_b$ where μ_s is a smooth polynomial spline fitted through the EXAFS region and μ_b is the background absorption, calculated according to the Victoreen formula.[52] For the present data, μ_s was determined by using a two region cubic spline, with spline points chosen to give the minimum Fourier transform intensity at low R (<1 Å). The EXAFS data were fitted to eq 2 by using a nonlinear least-squares algorithm. In eq 2, N

$$\chi(k) = \frac{N}{kR^2}\cdot S(k)\cdot F(k)\cdot\exp(-2k^2\sigma^2)\cdot\sin(2kR + \Phi(k)) \qquad (2)$$

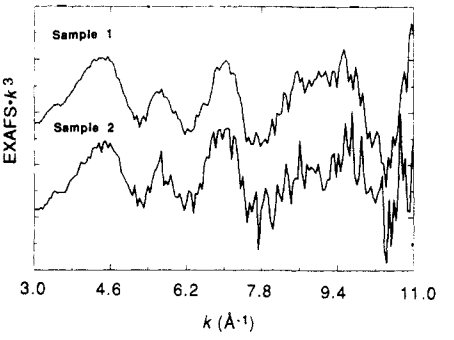

Figure 1. Unsmoothed, k^3 weighted EXAFS data for two OEC samples (S_1 state): top, sample 1, average of 17 scans and bottom, sample 2, average of 8 scans. Spectra are plotted on the same scale and have been displaced for clarity. Spacing between tick marks on vertical scale is 2.0.

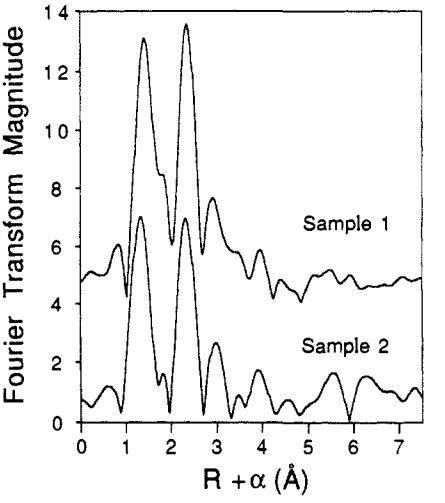

Figure 2. Fourier transforms of EXAFS data in Figure 1. Transforms calculated by using k^3 weighting for 3.5 Å^{-1} < k < 11.5 Å^{-1}. Spectra are plotted on the same vertical scale and displaced vertically for clarity: top, sample 1 and bottom, sample 2. The higher noise level for sample 2 (8 scans rather than 17 scans) is apparent in the high R signals for this sample.

is the number of scattering atoms, S is a scale factor, F is the intrinsic backscattering amplitude for a given absorber-scatterer pair, σ^2 is the mean square relative displacement in absorber–scatterer bond length, R, and Φ is a phase shift. Equation 2 represents the EXAFS for a shell consisting of a single type of scatterer at a single distance from the absorber. In modelling complex data such as that for the OEC, multiple (two or three) shells of scatterers, each having the form of eq 2, were refined simultaneously.

The amplitude, $F(k)$ and the phase $\Phi(k)$ are functions characteristic of a particular absorber–scatterer pair. Both ab initio and empirical parameters were used to describe these functions. Ab initio parameters[53] were calibrated by using a method similar to that described by Teo.[14e,54] In this procedure, eq 2 was fitted to the data for a structurally characterized model compound with S (independent of k), R, σ, and E_0 allowed to vary and N fixed at the crystallographic value. The values of S and E_0 which were determined in this manner were then held fixed in subsequent fits of the OEC EXAFS data. Empirical amplitude and phase parameters were determined by using a Fourier filtering procedure to isolate the EXAFS for a single shell, which was then decomposed into an amplitude and phase. In terms of eq 2, the empirical amplitude function is $S(k)\cdot F(k)$, while the phase function includes both $\Phi(k)$ and any correction term due to an incorrect choice of E_0. The change in disorder between model and unknown, $\Delta\sigma^2$, rather than an absolute σ, is determined in this method. Model compounds were $KMnO_4$ and $Mn^{III}(urea)_6$ for Mn–O and $Mn^{II}(imidazole)_6$ for Mn–N and Mn–C. As a good model for Mn–Mn EXAFS was not available, only ab initio parameters could be used for this shell. With these parameters, S and E_0 were set to 0.3 and −0.5 eV, respectively.[55]

(35) Cramer, S. P.; Tench, O.; Yocum, M.; George, G. N. *Nuclear Instr. Meth. Phys. Res.* **1988**, *586*, A226.

(36) Abbreviations used: H_2SALPS = *N,N'*-[1,1'-dithiobis(phenylene)]-bis(salicylideneaminato); H_2SALEN = bis(salicylideneaminato)ethylenediamine; 2-OH-SALPN = bis(salicylideneaminato)-2-OH-propylenediamine; H_2SALADHP = 1,3-dihydroxy-2-methyl-2-(salicylidene)propyleneamine; H_3DALAP = 1,6-bis(imino-2-hydroxyphenyl)-*p*-cresol-1,6-dialdehyde; H_2SALATHM = tris(hydroxymethyl)salicylideneaminato methane; H_2-5-Cl-SALAHP = 3-(5-Cl-salicylideneaminato)hydroxypropane; H_2SALPN = *N,N'*-bis(salicylideneaminato)propylenediamine; DPDP = *N,N'*-dipyridoxylethylenediamine-*N,N'*-diacetate-5,5'-bis(phosphate); TPP = dianion of *meso*-tetraphenylporphyrin; TMP = dianion of *meso*-tetramesitylporphyrin.

(37) Kessissoglou, D. P.; Butler, W. M.; Pecoraro, V. L. *Inorg. Chem.* **1987**, *26*, 451.

(38) Garrett, T. P. H.; Guss, J. M.; Freeman, H. C. *Acta Crystallogr.* **1983**, *C39*, 1027–1031.

(39) Bertraut, E. F.; Duc, T. Q.; Burlet, P.; Burlet, P.; Thomas, M.; Moreau, J. M. *Acta Crystallogr.* **1974**, *B30*, 2234.

(40) Kessissoglou, D. P.; Kirk, M. L.; Lah, M. S.; Li, X.; Hatfield, W.; Pecoraro, V. L. Manuscript in preparation.

(41) Pecoraro, V. L.; Li, X.; Baker, M. J.; Butler, W. M.; Bonadies, J. A. *Recl. Trav. Chim. Pays-Bas* **1987**, *106*, 221.

(42) Bonadies, J. A.; Kirk, M. L.; Lah, M. S.; Hatfield, W. M.; Pecoraro, V. L. *Inorg. Chem.* **1989**, *28*, 2037.

(43) Bonadies, J. A.; Maroney, M. J.; Pecoraro, V. L. *Inorg. Chem.* **1989**, *28*, 2044.

(44) Czernuszewicz, R. S.; Su, Y. O.; Stern, M. K.; Macor, K. A.; Kim, D.; Groves, J. T.; Spiro, T. G. *J. Am. Chem. Soc.* **1988**, *110*, 4158–4165.

(45) Aghabozorg, H.; Palenik, G. J.; Stoufer, R. C.; Summers, J. *Inorg. Chem.* **1982**, *21*, 3903–3907.

(46) Mikuriya, M.; Torihara, N.; Okawa, H.; Kida, S. *Bull. Chem. Soc. Jpn.* **1981**, *54*, 1063.

(47) Fackler, J. P.; Jr.; Avdeef, A. *Inorg. Chem.* **1974**, *13*, 1864.

(48) Camenzind, M. J.; Hollander, F. J.; Hill, C. L. *Inorg. Chem.* **1982**, *21*, 4301.

(49) Kessissoglou, D. P.; Butler, W. M.; Pecoraro, V. L. *J. Chem. Soc., Chem. Commun.* **1986**, 1253.

(50) Kessissoglou, D. P.; Li, X.; Butler, W. M.; Pecoraro, V. L. *Inorg. Chem.* **1987**, *26*, 2487.

(51) Larson, E. L.; Bonadies, J. A.; Pecoraro, V. L. Submitted to *Inorg. Chem.*

(52) *International Tables for X-ray Crystallography*, MacGillavry, C. H.; Rieck, G. D. Eds.; D. Reidel: Boston, 1985; Vol. III, pp 171–174.

(53) Teo, B. K.; Lee, P. A. *J. Am. Chem. Soc.* **1979**, *101*, 2815–2832.

(54) Teo, B. K.; Antonio, M. R.; Averill, B. A. *J. Am. Chem. Soc.* **1983**, *105*, 3751–3762.

Regardless of the source of the amplitude and phase parameters, fits to the OEC EXAFS data used three variable parameters per shell; N, R, and $\Delta\sigma^2$. In analyzing the protein EXAFS, N was fixed at different integer or half-integer values, and R and $\Delta\sigma^2$ were allowed to refine. In this way it was possible to determine the optimal value for N while retaining a minimum number of variable parameters. Identical structural parameters, within the estimated uncertainty, were obtained for empirical and theoretical parameters. Both the empirical and the calibrated ab initio parameters are dependent on the choice of model compound. However, the fact that we obtain the same structural results by using parameters derived from a variety of model compounds demonstrates that our results are independent of these minor phase and amplitude differences between models.

The current data have a sufficiently large signal-to-noise ratio that it was possible to use k^3 weighting for all analyses, including plots, Fourier transforms, and curve-fitting calculations. The k^3 weighting factor approximately corrects for the decrease in EXAFS amplitude at high k,[14a] thereby giving equal weight to the entire EXAFS spectrum.

For XANES analyses, the spectra were normalized by using a new procedure.[56] Rather than using different polynomials to model the pre-edge and post-edge regions, a *single* polynomial and scale factor were used. The scale factor and polynomial coefficients were adjusted so that the normalized data had the optimal agreement in a least-squares sense with tabulated X-ray absorption cross sections[57] both below and above the absorption edge. This procedure allows quantitative comparison of XANES spectra with an uncertainty of less than 5%.

Results

EXAFS. The k^3 weighted EXAFS data for the two different OEC samples are shown in Figure 1. The high signal-to-noise ratio and good reproducibility of these data are apparent—note that these data have not been smoothed. The higher quality of these data in comparison with earlier solution XAS studies of the OEC is attributable to the higher concentrations of Mn in our samples and the use of a solid-state detector array. Data of comparable signal-to-noise ratio have been reported recently by George et al. for the OEC in oriented photosynthetic membranes.[58] The Fourier transforms of the data in Figure 1 are shown in Figure 2. The Fourier transform of an EXAFS spectrum has peaks corresponding to each of the different shells of scatterers, with the peak positions shifted by typically −0.3 to −0.5 Å from the true absorber–scatterer distance due to the phase shift $\Phi(k)$ in eq 2.[59] The absence of spurious signals at higher R ($R > 4$ Å) again reflects the high quality of the present data.

Many of the features of the Fourier transforms are similar to those reported by Klein, Sauer, and co-workers.[15-21] We see three, and possibly four, peaks which are present above the noise level of the data. The first two peaks, corresponding to shells of atoms at distances of ca. 1.9 and 2.7 Å from the Mn, are identical with those reported in the most recent work by McDermott et al.[21b] In their earlier EXAFS studies, Klein, Sauer, and co-workers found that the 1.9-Å peak was split into two peaks.[18,20,21a,32] As discussed by Yachandra et al.,[20] these differences in the low R peak reflect the sensitivity of Fourier transforms to noise and incomplete background removal and are not necessarily indicative of any real difference in structure. In addition to the two main peaks, we also see smaller peaks corresponding to atoms at distances of ca. 3.3 and 4.5 Å from the Mn. The former was tentatively reported by Yachandra et al.[21a] for a spectrum obtained by averaging EXAFS data for S_1 and S_2 but was not detectable above the noise level of either the S_1 or S_2 data independently. The peak at 4.5 Å has not previously been noted.

These four peaks are independent of both the Fourier transform range and the window function used to define the EXAFS data used for transformation. This suggests that these peaks do not arise from transform artifacts (e.g., truncation). Other peaks (e.g., those at ca. 0.7, 1.8, and 3.5 Å) are dependent on the transform parameters and are therefore unlikely to represent real structural features.

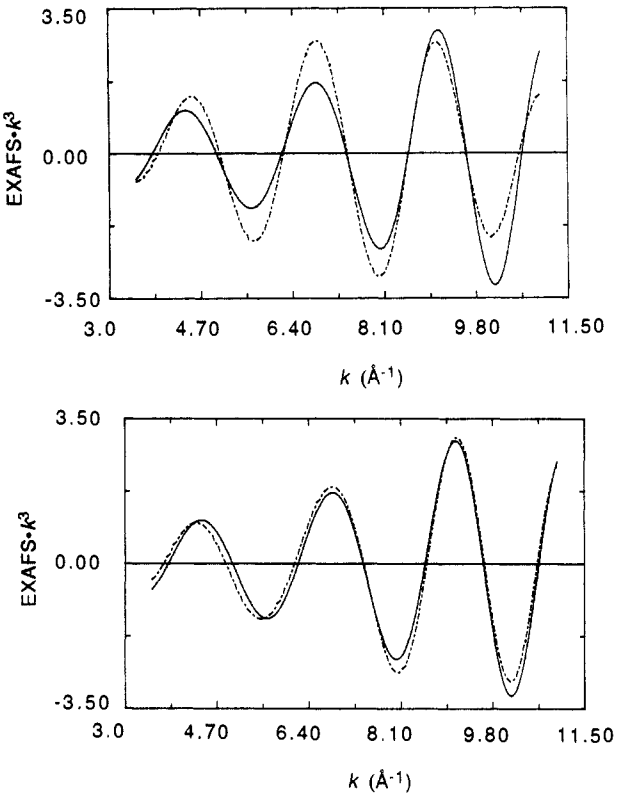

Figure 3. Best fit to filtered EXAFS corresponding to first Fourier transform peak (0.9 Å < R < 2.3 Å). Fit parameters given in Table II, solid line = fitted data and dashed line = best fit: (top) best one shell fit and (bottom) best two shell fit.

In our quantitative curve fitting analysis of the EXAFS data, we first proceeded by Fourier filtering the four different peaks and fitting each peak independently. While this procedure greatly simplifies the curve fitting analysis, it is possible that truncation effects arising from the Fourier filtering could perturb the results. To check for this possibility, we have repeated the fitting by using a range of different filter limits, including a filter consisting of the combined first and second shells and the unfiltered EXAFS data. The quantitative results are independent of filter; however, the sensitivity of the fits to the presence of atoms in the higher R shells is greatly reduced for the wide filters.

First Shell. EXAFS data for the first Fourier transform were filtered over the range 0.9 to 2.1–2.3 Å, and the data were fitted to eq 2 by using either Mn–O or Mn–N parameters. Comparable results were obtained for each set of parameters, with the principle difference being a slightly shorter distance when Mn–N parameters were used (ca. 1.88 Å for Mn–N, ca. 1.91 Å for Mn–O). The results that follow are discussed in terms of the Mn–O fits, since it is generally thought[1] that oxygenic ligands dominate the Mn coordination environment. We emphasize, however, that EXAFS cannot provide any direct information on the number, if any, of nitrogen ligands that are present.

The best single-shell fit to these data gives ca. two oxygens at 1.91 Å. This coordination number is too low, indicating either that there is substantial disorder in this shell or that more than one shell of ligands contribute to the first Fourier transform peak leading to destructive interference between the different contributions. The small σ^2 value for this shell suggests that disorder is not responsible for the low coordination number. Support for the multiple shell model is found in the fact that the filtered data can be well modelled by a fit incorporating two oxygens at 1.91 Å and two oxygens at 2.13 Å. These fitting results are summarized in Table II. In Figure 3 we compare the best one shell and two shell fits. Although the one shell fit is able to match the EXAFS

(55) These are typical of values found for other metal–metal EXAFS. See for example: Lindahl, P. A.; Teo, B.-K.; Orme-Johnson, W. H. *Inorg. Chem.* **1987**, *26*, 3912–3916.
(56) Waldo, G. S.; Penner-Hahn, J. E. Manuscript in preparation.
(57) McMaster, W. H.; Kerr Del Grande, N.; Millett, J. H.; Hubbel, J. H. *Compilation of X-ray Cross Sections*; UCRL-50174, Section II, Rev. 1.
(58) George, G. N.; Prince, R. C.; Cramer, S. P. *Science* **1989**, *243*, 789–791.
(59) Sayers, D. E.; Lytle, F. W.; Stern, E. A. *Phys. Rev. Lett.* **1971**, *27*, 1204.

Table II. Representative Curve Fitting Results for First Fourier Peak[a]

shell 1			shell 2			shell 3			
R	*N*	$\Delta\sigma^2$	*R*	*N*	$\Delta\sigma^2$	*R*	*N*	$\Delta\sigma^2$	F[b]
			1.92	(2)	−4.9				6.1
			1.92	(2)	−5.9	2.13	(2)	4.4	3.8
1.74	(1)	6.9	1.92	(2)	−7.5	2.12	(1)	−3.6	2.1
1.72	(1)	2.1	1.92	(2)	−6.4	2.08	(2)	18.9	1.6
1.71	(1)	2.1	1.91	(2)	−6.4	2.07	(3)	9.6	1.5

[a] Fits to filtered data corresponding to first Fourier peak (see text). All fits were calculated by using $Mn^{III}(urea)_6$ as a model compound. Coordination number (*N*) was fixed at the indicated integer values for refinements. Mn–O bond lengths (*R*) given in Å, Debye-Waller factors (σ^2) given as $Å^2 \times 10^3$. [b] Fit index *F* defined as $\{[(k^3\chi_{obs} - k^3\chi_{calc})^2/(N_{data} - N_{var})]^{1/2}\}/(k^3\chi_{max} - k^3\chi_{min}) \times 100\%$ where N_{data} and N_{var} are the number of data points and number of variables, respectively, and $\chi_{max} - \chi_{min}$ are the maximum and minimum observed values for filtered EXAFS data.

frequency reasonably well, both shells are required in order to reproduce the observed amplitude. It is also clear that the two shell fit does a good job of reproducing all of the features of the observed spectrum, suggesting that there is no requirement for a third shell of scatterers.

Klein, Sauer, and co-workers have reported[18,20,21,32] that the Mn nearest neighbors in the OEC are two oxygens (or nitrogens) at 1.75 Å and 2–3 oxygens (nitrogens) at 2.0–2.1 Å. We were unable to fit our data to a two shell model which includes a shell of oxygens at 1.75 Å. If a two shell refinement was started from a model having a shell of oxygens at 1.75 Å the final fit had either (a) the 1.9 and 2.1 Å result from above, (b) chemically unreasonable parameters (e.g., $R_{Mn-O} < 1.6$ Å), or (c) only one shell (i.e., the disorder parameter for one of the shells increases to an unreasonably large value, while the other shell refines to 1.9 Å). These results suggest that our samples do *not* contain a significant component of the 1.75 Å Mn–O distance reported previously. A similar conclusion was reached by George et al. in their study of oriented thylakoid membranes.[58]

Additional support for the absence of a significant 1.75 Å Mn–O component comes from a detailed analysis of the EXAFS amplitudes. Bunker has described a model-independent method for determining pair-distribution functions by using a cumulant expansion for describing the EXAFS amplitude.[60] In this procedure, one calculates the ratio of the EXAFS amplitudes, as determined by Fourier back-transformation, for the unknown and a model. The log of this ratio is fitted to a function $C_0 + C_2k^2 + C_4k^4 + \ldots$ where the C_i are related to the distribution of absorber–scatterer distances. For a narrow, symmetric distribution of bond lengths, only C_0 and C_2 are nonzero. More complex distributions, e.g., a two shell model, give rise to nonzero C_4 values. For the range of our data, simulations show that two shell models with shells at 1.9 and 2.1 Å give very small C_4 values, i.e., plots of log (amplitude ratio) vs k^2 are linear. Linear plots of log (amplitude ratio) vs k^2 are also obtained for the OEC EXAFS data, by using either $Mn^{II}(imidazole)_6$ or $Mn^{III}(urea)_6$ as the model. In marked contrast, simulations using scatterers at 1.75 and 2.15 Å give pronounced slope and curvature (C_4 comparable in magnitude to C_2). We were unable to reproduce the observed linearity by using any model that included a significant number (greater than roughly one per Mn atom) of oxygen atoms at 1.75 Å.

We emphasize that our fitting results do not permit us to exclude the possibility that there are some Mn–O distances at approximately 1.75 Å. Indeed, it is possible to include a shell of oxygen at 1.75 Å when three shells are refined simultaneously. This fit gives ca. a 2-fold improvement in quality of fit relative to a two shell fit. These three shell fits contribute little, however, to the structural characterization of the Mn site(s).

The number of degrees of freedom[14a] in the filtered EXAFS spectrum ($\Delta R \approx 1$ Å, $\Delta k \approx 10$ $Å^{-1}$) is ca. 6–7, thus a three shell fit with six variable parameters (*R* and $\Delta\sigma^2$ for each shell) is at best only slightly overdetermined. This suggests that three shell fits are unlikely to yield reliable structural parameters. As a typical example of this, a small change in one parameter for the three shell fits (the number of oxygens at 2.1 Å) results in large variations in the refined structural parameters (Table II). Similar sensitivity was not observed for two shell fits. A further difficulty with the three shell fits is the unusually large $\Delta\sigma^2$ values observed for the 1.75 Å shell, since $\Delta\sigma^2$ should decrease for shorter shells. We conclude from these observations that three shell fits cannot be used to determine the number of short Mn–O contacts in our samples.

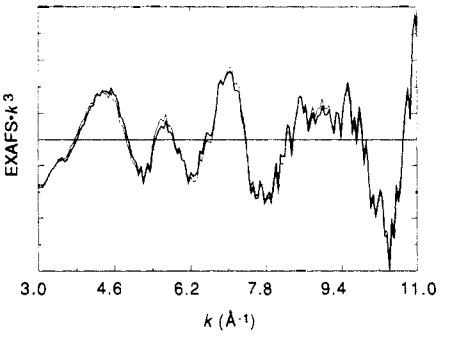

Figure 4. Effect of a single Cl^- at 2.3 Å on the OEC Mn EXAFS. Dark line = EXAFS data (average of 17 scans, k^3 weighting) of the OEC (S_1 state). Light line = same EXAFS data with calculated Mn–Cl scattering added.

As described previously, there is substantial evidence that Cl^- interacts with the OEC; however, there is at present no direct evidence for Cl^- coordination to Mn. Initial EXAFS results were interpreted as indicating that Cl^- could not be bound to Mn.[21a,32] However in a recent study, Klein, Sauer, and co-workers showed that the presence of one Cl^- per four Mn would not make a contribution which was above the noise level of the EXAFS data.[20] Given the higher quality of our EXAFS data, it was of interest to determine whether nondetectability of Cl^- still remained. To address this question, we calculated what changes would occur in the EXAFS if a single Cl^- per four Mn were present at 2.3 Å.[61] In Figure 4 we compare the measured OEC EXAFS data to a spectrum calculated by adding the simulated Mn–Cl EXAFS to the measured EXAFS spectrum. It is clear that the difference between these spectra is within the noise level of our data. When one considers that the simulation in Figure 4 is the optimal case for detectability, since a Cl could be present at a distance longer than 2.3 Å[49,50] and hence make an even smaller contribution to the EXAFS, it is clear that a substantial (perhaps 10-fold) improvement in signal-to-noise ratio is a minimum requirement for unambiguous detection of Mn–Cl EXAFS.

Second Shell. The second shell peak is well modelled by 1–1.5 Mn at 2.72 Å. The accuracy of this fit, in particular the accuracy of the coordination number, will be decreased if there are other non-Mn scatterers at the same distance which make substantial contributions to the EXAFS. In the case of the OEC, the only reasonable scatterers at 2.7 Å are carbon or chlorine. Two lines of evidence suggest that there is no substantial component of Mn–C EXAFS contributing to the 2.7 Å peak. No improvement (less than 10% decrease in F) was obtained for two shell fits (Mn + C) relative to one shell fits (Mn only). Furthermore, it is unlikely that the OEC contains structures which would give rise to a shell of atoms other than Mn at 2.7 Å. A survey of the Cambridge crystallographic data base suggests that 2.7 Å Mn–C distances are found only in five- and six-membered metallocycles such as $Mn(acac)_3$ and are thus unlikely to be present in the OEC. A Cl contribution to the 2.7 Å shell is structurally reasonable;

(60) Bunker, G. *Nucl. Instrum. Methods* **1983**, *207*, 437–444.

(61) 2.3 Å was chosen as a common Mn(III)–Cl bond length. Different Mn–Cl distances give slightly different simulated EXAFS spectra due to differing interference between Mn–Cl and Mn–(O/N) EXAFS; however, they do not affect our conclusions. Mn–Cl EXAFS was simulated as described in the text, by using ab initio EXAFS parameters.

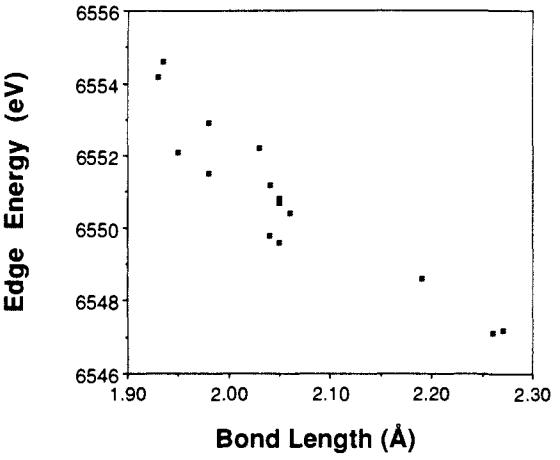

Figure 5. Edge energy vs Mn-ligand bond distance in Mn model compounds listed in Table I (including mixed-valence species). Mn(TMP)-OH is omitted since this complex is not crystallographically characterized.

however, any such contribution is likely to be extremely weak, particularly considering the disorder which is likely for such a long Mn-Cl interaction.

If the four Mn in the OEC had a single Mn-Mn distance of 2.7 Å, the average coordination number would be 0.5 (two atoms with a Mn-Mn coordination number of one, two atoms with a Mn-Mn coordination number of zero). Thus, the average coordination number of 1-1.5 Mn in the OEC indicates that there are most likely two or three Mn-Mn interactions at 2.7 Å. A somewhat larger number of Mn-Mn interactions (four or five), while less likely, could be consistent with our data if these interactions were characterized by substantial disorder. A smaller number, i.e., one Mn-Mn interaction of 2.7 Å, is not consistent with our data.

Third Shell. The third peak can be fitted with 0.5-1.0 Mn at 3.31 Å. This peak can be modelled equally well by using a Ca rather than Mn; however, Ca seems somewhat less likely since 3.3 Å is short for a Mn-Ca interaction. In contrast with the second shell, the fit to the third shell is substantially improved by including ca. one carbon at 3.55 Å. The presence of carbon scatterers at this distance is not surprising and is typical of distances seen for carboxylate, alkoxide, and phenoxide ligation. It was not possible, however, to obtain a good fit to the third shell by using carbon as the only scatterer. This suggests that there must be at least some contribution of Mn to the EXAFS at this distance; however, the presence of both Mn and C significantly decreases the precision of our curve fitting analysis. The observed Mn-Mn coordination number of 0.5-1.0 suggests that there are only one or two Mn-Mn interactions at 3.3 Å. A larger number of 3.3-Å Mn-Mn interactions cannot be excluded on the basis of the EXAFS data; however, it is difficult to imagine a plausible structure which has a substantially larger number of 3.3-Å Mn-Mn interactions and which is still consistent with the second shell EXAFS, since a four Mn structure can have at most six Mn-Mn interactions.

Fourth Shell. There is a fourth shell at ca. 4.35 Å. Although it is weak, this feature is present above the noise level in both data sets. This is a long distance to be detected by EXAFS; however, it is not without precedent. Freedman et al.[62] report tentative detection of a 3.9-Å Cu-Cu distance in metallothionein data measured at 130 K. Arbor et al. report readily detectable EXAFS for a 3.7-Å Fe-Fe interaction in nitrogenase data measured at 35 K.[63] As our data were measured at an even lower temperature (10 K), detection of such long distance interactions should be possible. The fourth shell can be fitted with ca. 0.5 Mn at 4.35 Å or 0.5 Ca at 4.3 Å. Given the long distance and the certainty that there are several other atoms (e.g., carbon) at a similar

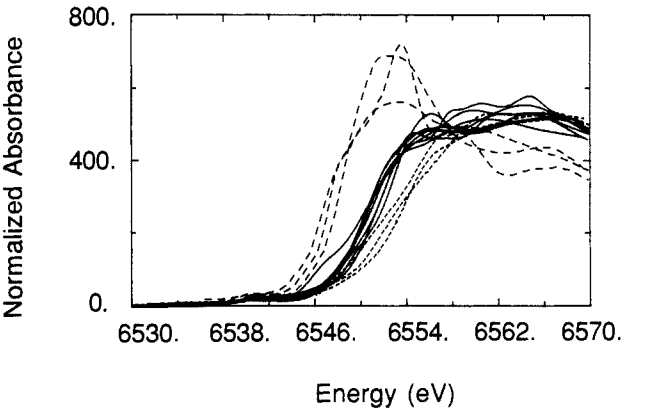

Figure 6. Plot of XANES for single oxidation state Mn model complexes listed in Table I: dashed line = Mn(II) complexes, solid line = Mn(III) complexes, dotted line = Mn(IV) complexes. In the interest of clarity, mixed-valence complexes are not plotted.

distance from the Mn, it is not possible at present to exclude alternate interpretations for this peak. Additional data will be required for unambiguous interpretation of this shell.

Near Edge Energy. It is well-known that edge energies tend to increase with increasing oxidation state,[16] a fact which has been used to assign Mn oxidation states in the OEC.[15-17,19-21,32] The X-ray absorption edge energies (defined as the first inflection point of the rising edge) for 16 Mn model complexes are provided in Table I. Although the *average* energies for the different oxidation states are clearly distinguished, it is obvious that the wide range of energies observed for a given oxidation state make it difficult to assign oxidation states unambiguously. It is particularly difficult to distinguish between Mn(III) and Mn(IV).

Part of the reason for this difficulty is illustrated in Figure 5, where we plot edge energy vs average Mn-ligand bond length for these complexes. It is clear that longer bond lengths, in addition to lower oxidation states, tend to be associated with lower edge energies. The degree of correlation evidenced in Figure 5 is rather surprising, given that we have made no attempt to account for chemical differences between compounds and have simply calculated an average first shell bond length. The correlation between bond length and energy has been discussed in theoretical[64] and experimental[65] studies of XANES and should give rise to an energy dependence of the form $E - E_0 \approx 1/R^2$. This correlation may account for much of the observed correlation between edge energy and oxidation state, since the average Mn-ligand distances are ca. 2.18, 2.02, and 1.93 Å for Mn(II), Mn(III), and Mn(IV), respectively.[66] Clearly, edge energies depend on both oxidation state and ligation. The above discussion suggests, however, that it is difficult to determine oxidation states unambiguously when relying solely on the first inflection point of the rising edge.

Near Edge Shape. The XANES spectra for the Mn model complexes are shown in Figure 6. In addition to changes in energy, it is obvious that the shape of the edge changes as oxidation state changes. Given these clear changes in edge shape, it should be possible to extract additional information from the XANES by fitting the entire edge rather than simply comparing edge energies.

To test this hypothesis, we attempted to fit the edges for a series of crystallographically characterized Mn(III/II/III) trinuclear complexes.[16,12,13,40] The analysis procedure was to fit the XANES of an unknown (e.g., the trinuclear complex) by a linear combination of two or more model XANES spectra. The only variable parameters were the fraction of each XANES spectrum that was included in the fit. The feasibility of this approach rests in part

(62) Freedman, J. H.; Powers, L.; Peisach, J. *Biochemistry* **1986**, *25*, 2342-2349.

(63) Arber, J. M.; Flood, A. C.; Garner, C. D.; Hassain, S. S.; Smith, B. E. *J. Phys. Colloque.* **1986**, *49*, C8-1159-C8-1163.

(64) Natoli, C. R. *Springer Ser. Chem. Phys.* **1983**, *27*, 43-56.

(65) Bianconi, A.; Congiu-Castellano, A.; Dell'Ariccia, M.; Giovannelli, A.; Buratini, E.; Durham, P. J. *Biochem. Biophys. Res. Commun.* **1985**, *131*, 98.

(66) These numbers were obtained from analysis of results reported in the Cambridge Crystallographic Structure Database. Penner-Hahn, J. E. Unpublished results.

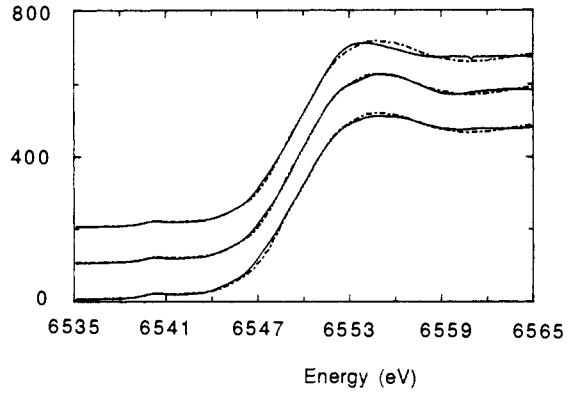

Figure 7. XANES spectra for the three trinuclear mixed-valence Mn complexes (see Table I) fit with Mn(II) and Mn(III) spectra. See text for details of fitting procedures: solid line = experimental data and dashed line = best fit of all models tried. For each trinuclear complex; the best fit was obtained by using $Mn^{II}(AcO)_2(H_2O)_2$ and $Na\{Mn^{III}$-[(2-OH)-5-Cl-SALPN]$\}_2$ as standards.

on our ability to normalize XANES spectra precisely. As described above, our new normalization procedure gives an uncertainty of less than 5% in normalized intensity, as judged by the agreement which we observe between spectra for the same compound measured under different conditions.

For the Mn(III/II/III) trinuclear complexes, good fits could only be obtained by using a Mn(II) and a Mn(III) model (Figure 7). Other combinations, e.g., Mn(II)/(II) or Mn(III)/(III) gave a fit that was a factor of 2–3 worse. Most importantly, regardless of the Mn(II) and Mn(III) models used, the ratio of Mn(II): Mn(III) was ca. 1:2 (37 ± 8% Mn(II)). As a further check, the Mn(III)–Na(I)–Mn(III) heterotrinuclear cluster $Na[Mn(2\text{-}OH\text{-}SALPN)(OAc)_2]_2$, which has a structure similar to the mixed-valence trinuclear species, could be fit by Mn(III) edges alone. If a Mn(II) component was included when fitting this complex, its amplitude refined to zero.

We conclude that, at least for a mixture of Mn(II) and Mn(III), this analysis procedure provides oxidation state information which is accurate to within ca. 10%, *independent of the Mn(II) and Mn(III) standards which are used.* A more conventional analysis, based solely on the energy of the first inflection point, would only be able to determine that the average oxidation state lies between Mn(II) and Mn(III). The somewhat surprising reliability of our fitting procedure derives from the fact that we utilize not only the energy but also the shape of the XANES spectrum. For the compounds which we have examined, shape rather than edge energy appears to be the feature most characteristic of a particular oxidation state.

OEC Near Edge Structure. The XANES spectrum of the OEC is shown in Figure 8. The edge energy is indicative of an average oxidation state of Mn(III), consistent with the conclusions of Klein, Sauer, and co-workers. However, upon comparison of Figures 7 and 8, the edge for the OEC appears noticeably broader than the edges for any of the model compounds. This suggests that the OEC (at least in the S_1 state) contains several different Mn environments. The edge fitting analyses for the OEC are summarized in Table III. The OEC edge could be modelled successfully only by including Mn(II), Mn(III), and Mn(IV) models. This is illustrated graphically in Figure 8. Although the ratio of Mn(III):Mn(IV) was dependent on the choice of models, we consistently obtained 15–25% Mn(II) regardless of the combination of models used. This amount of Mn(II), 0.225–0.375 mM, is well above the detectable limits for adventitious Mn(II). These results are consistent with an oxidation state composition of 1:2:1 or 1:1:2 for Mn(II):Mn(III):Mn(IV). Of these, the former is more attractive, since it gives an average oxidation state of Mn(III) and accounts for the lack of an EPR signal for the S_1 state. As we discussed above, there are many factors other than oxidation state which can affect the appearance of XANES spectra. It is important to emphasize that we cannot rule out the possibility that some other structural feature, perhaps unusually long or short Mn bond lengths, could account for the observed OEC edge.

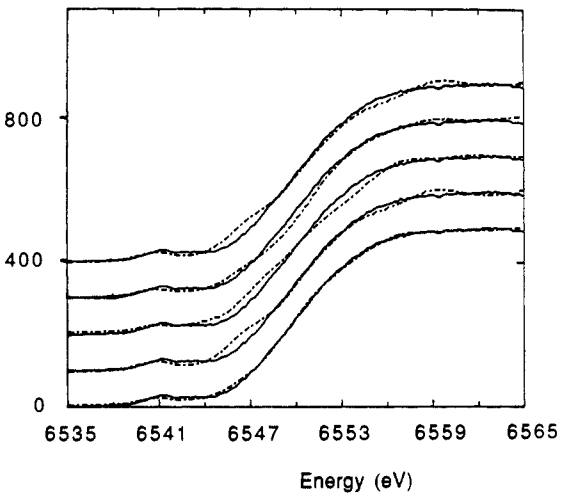

Figure 8. OEC XANES spectra fit with a combination of Mn models: solid line = OEC data and dashed lines = best fits obtained for the different oxidation state models. For each oxidation state model, the data were fit by using all of the spectra of the appropriate oxidation states. The oxidation state models are from top Mn(II) + Mn(III), Mn(III) + Mn(III), Mn(II) + Mn(IV), Mn(III) + Mn(IV), and Mn(II) + Mn(III) + Mn(IV). The best fits were obtained by using $[Mn(SALPS)_2]_2$ + Mn(TMP)(Cl), Mn(TMP)(Cl) + $\{Mn[(2\text{-}OH)\text{-}5\text{-}Cl\text{-}SALPN]\}_2$, $[Mn(SALPS)_2]_2$ + $Mn(SALADHP)_2$; [Mn(TMP)(Cl) + $Mn(TPP)(OMe)_2$, and $Mn(AcO)_2(H_2O)_2$ + Mn(TMP)(Cl) + $Mn(SALADHP)_2$, respectively.

Table III. Edge Fitting Results

model[a]	% deviation[b]	% Mn(II)[c]
Mixed-Valence Trimers [Mn_3(III/II/III)]		
II + II	18.0	
III + III	11.1	
II + III	3.6	38 (30–50)
OEC		
III + III	4.2	
III + IV	4.2	
II + III	3.9	12 (2–25)
II + IV	2.8	30 (23–35)
III + III + III	3.9	
II + III + III	3.2	12 (3–24)
II + III + IV	2.0	23 (17–32)

[a] Roman numerals indicate the formal oxidation states of the models which were included in the fits. [b] Calculated as $\{[(\mu_{obs} - \mu_{calc})^2/(N_{data} - N_{var})]^{1/2}\}$/(edge jump) where μ_{obs} and μ_{calc} are observed and calculated edge spectrum, N_{data} is the number of data points, N_{var} is the number of variable parameters (i.e., the number of files used in the fit), and (edge jump) is the change in absorbance, μ, across the edge. Value reported is the average of the values obtained for all of the fits with use of a specific oxidation state model. [c] Average percent Mn(II) obtained for all of the fits with use of a specific oxidation state model. Values in parentheses are the range of % Mn(II) obtained for *all* of the fits with use of a given oxidation state model.

Que and co-workers have shown that the intensity of the Fe 1s → 3d transition can be correlated with the distortion of the Fe site from octahedral symmetry.[67] For Fe(III), the normalized 1s → 3d peak areas (in units of 10^{-2} eV) are 6–9 for six-coordinate, 12–19 for five-coordinate, and 23–25 for four-coordinate Fe(III).[67] We find comparable values for our Mn model complexes. The 1s → 3d region of the OEC XANES spectrum has a normalized area, on this scale, of 14.4. This is more intense than the 1s → 3d transition observed for the six-coordinate Mn models and suggests that some of the Mn sites are distorted from octahedral symmetry. The most likely distortions are five-coordinate sites and/or the presence of short μ-oxo bridges.

(67) Roe, A. L.; Scheider, D. J.; Mayer, R. J.; Pyrz, J. W.; Widom, J.; Que, L., Jr. *J. Am. Chem. Soc.* **1984**, *106*, 1676–1681.

Discussion

There are four principle questions that we hoped to address in this study: (1) active site nuclearity, (2) structural requirements of the cluster(s), (3) ligands to the manganese, and (4) oxidation state of the manganese in the S_1 level. Each point will be summarized below.

Metal Nuclearity. Given the high quality of data on both the model and biological samples, we can now evaluate structural and oxidation state proposals for the OEC. Models which invoke tetranuclear,[9,68] mononuclear/dinuclear,[11] mononuclear/trinuclear,[12,13] and dimers of dimers[17,1c] have all appeared within the last 2 years attesting to the considerable controversy in this field. Given the complexity of the system, it is unlikely that EXAFS alone will ever provide an unambiguous description of the OEC structure. It is important, however, to examine these models in the light of our current data with the goal of determining which, if any, possibilities can be excluded. The two most widely discussed tetranuclear models have been forwarded by Brudvig and Crabtree[9] and by Christou.[68] The Brudvig–Crabtree proposal invokes an elongated Mn_4O_4 cubane that is sequentially oxidized and, in the higher S states, converts to an Mn_4O_6 adamantane structure.[69] The Christou proposal, based on a series of synthetic models,[70-72] relies on an Mn_4O_2 core of a bufferfly cluster which in the higher S states forms a cubane-like structure. The EXAFS data presented herein are clearly inconsistent with either a symmetric cubane or a butterfly structure. The cubane model is ruled out based on the heterogeneous nature of both the XANES and EXAFS. A cubane would be expected to have a relatively sharp edge, since the Mn would all be in similar environments, and a Mn–Mn coordination number of three, in contrast with our data. Klein, Sauer, and co-workers have drawn a similar conclusion from analysis of the Mn–Mn coordination number in their EXAFS data. If the axial elongation in the Brudvig–Crabtree model[9] was long enough that four of the six Mn–Mn distances increased to 3.3 Å, it could be consistent with our data; however, such a structure would be inconsistent with the orientational asymmetry reported by George et al. for the 3.3 Å Mn–Mn.[58]

The butterfly structures which have been reported to date[70-72] are also ruled out by the 2.7 Å Mn–Mn coordination number. The butterfly complexes have a single 2.7 Å distance, giving an average Mn–Mn coordination number of 0.5, as compared with our fits which give an average Mn–Mn coordination number of 1–1.5 for the OEC. Although these two idealized structures are inconsistent with our data, it is important to note that EXAFS data alone cannot distinguish between other structural possibilities. Among the structures consistent with our data are distorted tetranuclear clusters (including distorted versions of the cubane or the butterfly models) or structures such as a dimer of dimers or a mononuclear/trinuclear organization.

The structural possibilities can be delimited further if one utilizes the EPR spectral data and interpretations of Hansson et al.[11] and the finding[20,21,32] that the S_1 and S_2 states have identical EXAFS spectra. Hansson et al. have suggested that the $g \approx 4$ signal comes from a mononuclear Mn(IV) ion. *If this signal does indeed come from a mononuclear center*, then the EXAFS data are only consistent with a mononuclear/trinuclear formulation for the manganese. We can state this conclusively for the following reasons. Klein, Sauer, and co-workers report that the EXAFS of S_1 and S_2 are identical,[20,21,32] which allows us to use our structural data for S_1 to evaluate the structure of S_2. In particular, this implies that S_2, like S_1, has a minimum coordination number of 1–1.5 for the 2.7 Å Mn–Mn shell. The importance of this observation rests on the fact that all examples of multinuclear manganese complexes in which the Mn–Mn separation is 2.7 Å exhibit strong magnetic coupling between ions. Since the $g \approx 4$ signal is required to come from an isolated Mn(IV) in the Hansson model, this manganese cannot be at 2.7 Å from another manganese ion. Therefore, at least one of the remaining three manganese atoms must have two Mn neighbors at 2.7 Å in order to account for the observed Mn–Mn coordination number of 1–1.5. This necessitates a trinuclear cluster. This analysis does not require that the 3.3 Å distance be associated with manganese; however, if the 3.3 Å feature does arise from a Mn–Mn interaction, one might expect in this model a bent cluster with a central manganese atom separated from two terminal manganese by 2.7 Å and the terminal manganese separated by 3.3 Å.

Structural Constraints on the Manganese. We can also comment on the core structural constraints for the manganese ions. Previously the short 1.75 Å Mn–(N,O) and 2.71 Å Mn–Mn distances were taken as evidence for a di-μ-oxo Mn(IV/IV) or Mn(III/IV) formulation since other bridging ligands give longer Mn–O distances. The reported coordination numbers require an average of two μ-oxo bridges per Mn.[13,20,21,32] Our finding that there is no well-defined shell at a short Mn–(N,O) distance indicates that there need not be *short* oxo bridges; however, it does not rule out the possibility of μ-oxo bridges at a longer distance. In fact, many of the μ-oxo bridges which have been characterized[51,70,73-77] for Mn complexes have Mn–O distances in the range of 1.83–1.9 Å, consistent with our data. In addition, other bridging structures, such as μ-hydroxo or μ-alkoxo, would also be consistent with our data. The OEC structure may in fact have a variety of different bridging ligands—this would be consistent with the apparent spread in first shell bond lengths.

The second shell Mn–Mn distance of 2.71 Å indicates that at least two pairs of manganese are linked by two or more single-atom bridges per pair. In the Mn clusters which have been structurally characterized to date, 2.7 Å Mn–Mn distances have been associated with di-μ-oxo bridges, while μ-alkoxo-bridged complexes give Mn–Mn distances of 3.0 Å or longer. However, the recent report[78] of a 2.296 Å Mn–Mn distance for a tri-μ-oxo dimer demonstrates that a considerable range of Mn–Mn distances are accessible. In particular, the tri-μ-oxo structure suggests that if a tri-μ-alkoxo species could be prepared, it would have a Mn–Mn distance similar to that found in the OEC.

The third shell distance of 3.3 Å is typical of those seen for carboxylato-bridged complexes. This is consistent with the prevalence of carboxylato residues in the OEC proteins; however, other bridging structures (i.e., oxo, alkoxo, or phenoxo) are also possible.

The intensity of the $1s \rightarrow 3d$ transition is typical of manganese in a noncentrosymmetric environment.[67,79] This could be achieved by distortions of the manganese coordination sphere (i.e., the presence of oxo ligands) or by lowering the coordination number of some of the manganese from six to five. We are unable at this point to distinguish between these possibilities.

Calcium and Chloride in the OEC. We have preliminary evidence for a new Mn–metal interaction at ≈4.35 Å. This could be either another manganese atom or, even more intriguing, a calcium ion. In addition to the absolute requirement for calcium in photosynthetic oxygen evolution, there is further biological precedent for Mn–Ca centers. For example, concanavalin A has a heterodinuclear metal binding site composed of a Mn(II) linked via two carboxylate groups to a Ca(II) ion with a Mn–Ca sepa-

(68) Vincent, J. B.; Christou, G. *Inorg. Chim. Acta* **1987**, *136*, L41.
(69) Wieghardt, K.; Bossek, V.; Gebert, W. *Angew Chem. Int. Ed. Engl.* **1983**, *22*, 328.
(70) Bashkin, J. S.; Chang, H.-R.; Streib, W. E.; Huffman, J. C.; Hendrickson, D. N.; Christou, G. *J. Am. Chem. Soc.* **1987**, *109*, 6502.
(71) Vincent, J. B.; Christams, C.; Huffman, J. C.; Christou, G.; Chang, H.-R.; Hendrickson, D. N. *J. Chem. Soc., Chem. Commun.* **1987**, 236.
(72) Christmas, C.; Vincent, J. B.; Huffman, J. C.; Christou, G.; Chang, H.-R.; Hendrickson, D. N. *J. Chem. Soc., Chem. Commun.* **1987**, 1303.
(73) Pecoraro, V. L.; Butler, W. M. *Acta Crystallogr.* **1986**, *C42*, 1151.
(74) Kulawiee, R. J.; Crabtree, R. H.; Brudvig, G. W.; Schulte, G. K. *Inorg. Chem.* **1988**, *27*, 1311.
(75) Collins, M. A.; Hodgson, D. J.; Michelsen, K.; Towle, D. K. *J. Chem. Soc., Chem. Commun.* **1987**, 1659.
(76) Plaskin, P. M.; Stouffer, R. C.; Mathew, M.; Palenik, G. J. *J. Am. Chem. Soc.* **1972**, *94*, 2121.
(77) Mashen, H. S.; Waters, T. W. *J. Chem. Soc., Chem. Commun.* **1973**, 760.
(78) Wieghardt, K.; Bossek, U.; Nuber, B.; Weiss, J.; Bonvoisin, J.; Corbella, M.; Vitols, S. E.; Girerd, J. J. *J. Am. Chem. Soc.* **1988**, *110*, 7392–7411.
(79) Shulman, R. G.; Eisenberger, P.; Blumberg, W. E.; Stombaugh, N. A. *Proc. Natl. Acad. Sci. U.S.A.* **1975**, *72*, 4003–4007.

ration of 4.3 Å.[80] The synthetic compound $CaNa_2MnDPDP \cdot 2lH_2O$ exhibits a Mn(II)–Ca separation of ≈4.4 Å with a bidentate carboxylate forming a μ-carboxylato oxygen bridge between the metals.[81] Future experiments, designed to address the possibility that the OEC manganese cluster may contain calcium, or at least have a calcium ion in close proximity, are in progress.

As for chloride ligation, we estimate that *at least* another order of magnitude increase in signal to noise is required to characterize definitively the Mn–Cl interaction. Mn EXAFS is thus not likely to be a useful technique for determining whether or not a single Cl is coordinated to a multimetal center, although Cl EXAFS could be useful in this regard.

Metal Oxidation States. As discussed, we have developed a new XANES analysis procedure in which we fit the entire XANES spectrum rather than simply comparing edge energies. This method appears to be both accurate and robust when applied to crystallographically characterized Mn complexes.

Our best fit results for the OEC suggest a formal oxidation state of $Mn(II)Mn(III)_2Mn(IV)$ or $Mn(II)Mn(III)Mn(IV)_2$. Both of these correspond well with previous reports of an average oxidation state of Mn(III) for S_1. This mixed-valence formulation is a reflection of the fact that the OEC edge occurs at an energy characteristic of Mn(III) but is broader than expected for a Mn(III) XANES spectrum. This is exactly what would be expected for a Mn(II/III/IV) mixed-valence species. It is important to bear in mind, however, that unusual coordination environments (for example, a Mn(III) which had a "Mn(II)-like" XANES spectrum) could account for the OEC XANES spectrum. However, until such models are found, we tentatively suggest that the S_1 oxidation level of the OEC contains Mn(II), Mn(III), and Mn(IV).

Given our discussion of possible cluster types, the known spectroscopic properties of the OEC, and our tentative oxidation state assignment, we can now speculate as to the overall organization of manganese in the OEC. The S_1 level is EPR silent. This is consistent with the $Mn(II)Mn(III)_2Mn(IV)$ oxidation state assignment if the Mn(II) and Mn(IV) ions are contained within the same cluster. Such a structure is without precedent in Mn coordination chemistry; however, there *are* examples of mixed-valence clusters in which the metal oxidation states differ by two, even though there are stable intermediate oxidation levels available.[82] Grouping the Mn(II) and Mn(IV) together into an Mn(II/III/IV) cluster would be consistent with the trinuclear proposal, and the remaining mononuclear Mn(III) would also be EPR silent as required for S_1. Oxidation of the enzyme would result in either an Mn(III/III/IV) cluster [$S = 1/2$, $g = 2$ multiline] with a mononuclear Mn(III) [EPR silent] or an Mn(II/III/IV) cluster [EPR silent] with a mononuclear Mn(IV) [$S = 3/2$, $g \approx 4$].

A more conventional oxidation state assignment still consistent with the EXAFS and EPR results would formulate S_1 as a Mn(III/III/III) trimer plus a Mn(III) monomer. If this assignment is correct, our XANES data indicate that one or more of the Mn ions must have an unusually distorted environment in order to account for the observed breadth of the OEC XANES spectrum. Thus, either oxidation state model requires that the OEC Mn environment be significantly more heterogeneous than has been considered in the models proposed to date. This conclusion is consistent with George et al.'s recent polarized EXAFS measurements for oriented thylakoid membranes showing relatively low symmetry for the Mn site(s).[58] Additional experiments aimed at further characterizing the Mn structure are in progress.

Acknowledgment. This work was supported in part by the National Institutes of Health (Grants GM-38047 to J.E.P.H. and GM-39406 to V.L.P.), the National Science Foundation (DCB-85-15932 to C.F.Y.), the U.S. Department of Agriculture (CRG0-88-37130-3546 to C.F.Y.), the G.D. Searle Family and Chicago Community Trust (Biomedical Research Scholar Award to V.L.P.), and the Camille and Henry Dreyfus Foundation (Distinguished Young Faculty Award to J.E.P.H.). X-ray absorption measurements were made at the Stanford Synchrotron Radiation Laboratory, which is supported by the U.S. Department of Energy, Office of Basic Energy Sciences, and the National Institutes of Health, Biotechnology Resource Program, Division of Research Resources. We thank Dr. S. P. Cramer for loan of the Ge detector array and Drs. S. P. Cramer, G. N. George, and R. Prince for communicating results prior to publication.

(80) Hardman, K. D.; Ainsworth, C. F. *Biochemistry* **1972**, *11*, 4910.
(81) Rockledge, S. M.; Cacheris, W. P.; Quay, S. C.; Hahn, F. E.; Raymond, K. N. *Inorg. Chem.* **1989**, *28*, 477.
(82) For example, see: Evans, J.; Gauntlett, J. T.; Levason, W. *Inorg. Chem.* **1988**, *27*, 4523–4524. Dulebohn, J. I.; Ward, D. L.; Nocera, D. G. *J. Am. Chem. Soc.* **1988**, *110*, 4054–4056, and references therein.